PROSTHETICS

The Hannes hand prosthesis replicates the key biological properties of the human hand

M. Laffranchi[1]*, N. Boccardo[1], S. Traverso[1], L. Lombardi[1], M. Canepa[1], A. Lince[1], M. Semprini[1], J. A. Saglia[1], A. Naceri[2], R. Sacchetti[3], E. Gruppioni[3], L. De Michieli[1]

Replacing the human hand with artificial devices of equal capability and effectiveness is a long-standing challenge. Even the most advanced hand prostheses, which have several active degrees of freedom controlled by the electrical signals of the stump's residual muscles, do not achieve the complexity, dexterity, and adaptability of the human hand. Thus, prosthesis abandonment rate remains high due to poor embodiment. Here, we report a prosthetic hand called Hannes that incorporates key biomimetic properties that make this prosthesis uniquely similar to a human hand. By means of an holistic design approach and through extensive codevelopment work involving researchers, patients, orthopaedists, and industrial designers, our proposed device simultaneously achieves accurate anthropomorphism, biomimetic performance, and human-like grasping behavior that outperform what is required in the execution of activities of daily living (ADLs). To evaluate the effectiveness and usability of Hannes, pilot trials on amputees were performed. Tests and questionnaires were used before and after a period of about 2 weeks, in which amputees could autonomously use Hannes domestically to perform ADLs. Last, experiments were conducted to validate Hannes's high performance and the human likeness of its grasping behavior. Although Hannes's speed is still lower than that achieved by the human hand, our experiments showed improved performance compared with existing research or commercial devices.

INTRODUCTION

Until recently, upper limb prosthetic systems were meant as tools rather than replacements of a missing arm or hand. The main reasons for this implementation were due to technological limiting factors that did not permit the restoration of the full functionalities of a missing limb. This is the case for traditional body-powered prosthetic devices based on split hooks, so-called prehensors, and more advanced myoelectric hands (*1*–*7*). As a main consequence, the drawbacks of such solutions lead to a substantial rate of abandonment of upper limb prostheses, which is one of the main obstacles that researchers in the field attempt to overcome (*8*, *9*).

Several studies have been carried out to determine the key factors that characterize the behavior and properties of the human hand as a guide to achieve a truly bioinspired prosthetic device; these factors are as follows: (i) anthropomorphic-related features, which include kinematics, size, weight, and appearance (*4*, *10*, *11*); (ii) performance such as speed, force, and dexterity (*10*, *12*); and (iii) robust and synergistic grasping (*13*–*18*). To effectively replicate the latter two aspects in a prosthesis, biomimetic motion velocity levels should be combined with an appropriate grip force: The digits should be able to move with a suitable speed and exert a sufficient grasp strength to make the device effective in the execution of activities of daily living (ADLs) (*5*). In addition, the digits should be controllable with suitable precision and responsiveness to enable proper usage and dexterity (*12*), which are also among the most basic requirements for permitting embodiment (*10*, *15*, *19*, *20*). These latter characteristics are strongly correlated with a variety of biomimetic properties beyond good engineering practice (*21*), including excellent similarity with the kinematic model and behavior of the human hand (*15*), human-like joint angular coordination, and, of course, robustness. Extensive research has been carried out on the sensorimotor system of the human hand and, specifically, on the control of the temporal and spatial coordination of the digit force, muscle, and joint movements (*17*, *22*). Principal components analysis (PCA) was used for exploring different hand patterns during grasping of several objects. This technique essentially allows the reduction of a large set of hand motor variables into a smaller set of principal components (PCs) representing the majority of these variables. With respect to this method, it was discovered that the kinematic synergistic behavior of the human hand during grasping is such that only the first two PCs are sufficient to classify and reconstruct hand postures at 80% of the variance, with a predominance of the first synergy among other PCs (*23*, *24*). Therefore, nature suggests that replicating grasping movements as combinations of synergistic motion patterns is another crucial factor that determines high levels of biomimicry and may ultimately lead to proficient execution of ADLs. These insights led scientists to develop systems that could intrinsically implement these synergies through ad hoc designs based on underactuation and, in some cases, mechanical compliance that intrinsically adapts the device's configuration during the interaction with the environment (*14*, *25*–*30*).

Nevertheless, the most advanced anthropomorphic robotic hands (*25*, *31*–*33*) or research prostheses (*2*, *10*, *14*, *30*, *34*, *35*) do not meet the weight, size, and/or power demands required for practical use (*36*). In the last decade, however, a few prosthetic devices have made an attempt to approach the functional and physical properties of a human hand, trying to satisfy the increasing need for function and "form" in one device (*8*). To replicate the form factor accurately, unconventional research approaches focus on the use of three-dimensional (3D) scanning of the contralateral limb and additive manufacturing techniques (*37*). Nevertheless, among several devices, the most successful implementations are represented by the Michelangelo and the BeBionic hands by Ottobock (*38*, *39*), the iLimb from Ossür (*40*), and the Vincent hand from Vincent systems (*41*). Although these devices resemble a human hand in their appearance

[1]Rehab Technologies, Istituto Italiano di Tecnologia, Via Morego, 30, 16163 Genova, Italy. [2]Advanced Robotics, Istituto Italiano di Tecnologia, Via Morego, 30, 16163 Genova, Italy. [3]Centro Protesi INAIL, Istituto Nazionale per l'Assicurazione contro gli Infortuni sul Lavoro, Via Rabuina 14, 40054, Vigorso di Budrio (BO) Italy.
*Corresponding author. Email: matteo.laffranchi@iit.it

and provide reasonably functional performances, the devices still do not incorporate several of the abovementioned fundamental properties of a human hand. The adaptability of these devices to different shapes and force distributions among the fingers is typically limited to static grasping, which results in an ineffective and unnaturally low grasp robustness (*11*, *42*), particularly when the grasped object is perturbed and/or moves within the prosthetic hand. The main reason for this limitation is that these devices are designed with traditional robotic "stiff" approaches, where the adaptability of the hand during an interaction relies on feedback control that hardly implements the high interaction ability typical of a human hand. Furthermore, the kinematics of these prostheses represent a gross simplification of that of a real hand, resulting in low levels of anthropomorphism. For some devices, the approximations include the suppression of some critical degrees of freedom (DOFs). For example, in the Michelangelo hand, only the metacarpophalangeal (MCP) joint is responsible for flexing or extending each of the fingers, whereas other devices do not include finger abduction/adduction. Similarly, in other poly-articulated hands, such as the BeBionic hand, the joints of each finger are coupled by a linear kinematic relationship that governs the coordination of the fingers' joints (*4*). These approximations in poly-articulated prostheses make the grasp and interaction much less effective, adaptable, and robust than the grasp and interaction of their biological counterpart: adaptable grasping increases the contact area and therefore the manipulation stability (*43*). Such design choices have further implications for the capability of implementing human-like movements and an appropriate synergic coordination between the joints: It follows that the overall biomimicry of such systems remains rather limited. Researchers have attempted to solve these issues by developing self-adapting mechanism concepts such as the KIT hand by Karlsruhe Institute of Technology (*35*) and the SoftHand by University of Pisa and Istituto Italiano di Tecnologia (*25*); nevertheless, the performance of these devices is far from the levels required to perform ADLs, resulting in limited usability.

In particular, researchers have advocated that the design approach should involve trade-offs among biomimetic performance, human-like grasping behavior, and anthropomorphism (*5*, *10*, *44*, *45*); however, we assert that these properties should all be included and follow an uncompromising holistic design approach that is paramount for achieving effective limb replacements with high potential of embodiment (*9*).

We propose a prosthetic hand called Hannes that incorporates high levels of biomimicry through the concurrence of anthropomorphism, performance, and functionality, which lead to better performance compared with other existing research and commercial prosthetic devices. This result was achieved by organically involving researchers, patients, orthopaedists, and industrial designers in a codesign process. Last, we perform a thorough evaluation of the device through laboratory tests and clinical trials on amputated participants.

RESULTS

System overview

Hannes consists of three main interacting physical components: a myoelectric poly-articulated prosthetic hand that exploits a differential underactuated mechanism; a passive flexion-extension (F/E) wrist module; and a myoelectric interface/controller that includes two surface electromyographic (sEMG) sensors, battery pack, and control electronics, as shown in Fig. 1A. These three components have been developed to realize anthropomorphism, biomimetic performance, and human-like grasping, which have been demonstrated in previous studies to be key aspects that determine the overall "goodness" of a prosthesis (*4*, *5*, *8*, *10*–*12*, *15*–*17*, *19*, *22*, *24*). These characteristics have been implemented using a holistic biomimetic design approach as shown in Fig. 2 and Movie 1.

Hannes's high anthropomorphism

Hannes is shown in Fig. 1B. Figure 3A shows the dimensions, kinematics, and ranges of motion (ROMs) of Hannes in direct comparison with a 50th percentile human hand used as reference for the design (*46*); see also table S1 for details. Figure 3A shows the extremely high anthropomorphism of Hannes: A maximum discrepancy of 4.8% can be observed in the proximal-intermediate diameter of the middle finger, demonstrating the exceptionally high resemblance with the reference hand model. Regarding the kinematics, Fig. 3B shows that all finger DOFs are implemented except the distal interphalangeal (DIP) joint, which is omitted and set to a fixed angle because of a design trade-off between functionality and the complexity of implementation. The thumb exhibits different kinematics such that the interphalangeal (IP) and MCP joints are locked, whereas abduction is actuated and rotation is passive.

Last, for a comprehensive comparison, Fig. 3C shows the angular excursions of Hannes's DOFs compared with the DOFs of the human hand and the Michelangelo prosthesis, which has been used as the gold standard due to its advanced anthropomorphism compared with that of other existing prosthetic hands (*4*, *38*). Apart from the locked DIP joints, Hannes's ROMs are, overall, close to those of the human hand and substantially more biomimetic than those of the Michelangelo prosthesis.

Passive wrist elasticity for enhanced adaptability

Another main component of Hannes is the passive F/E wrist on the proximal part of the hand. This module naturally conforms to its F/E based on interaction forces, and it has been demonstrated to achieve grasp robustness and adaptability to the task being executed, as shown in Movie 2. At the base of the wrist, a quick release system replicates the "de facto" standard produced by Ottobock and is manufactured to permit the connection of Hannes to the socket and achieve an electrical connection with the controller. This component additionally allows passive prono-supination of the hand.

Intuitive interface and direct strategies for seamless grasping

Regarding control and interfacing, we decided to adopt direct EMG control for the sake of reliability, robustness, and practicality, leaving the implementation of the aforementioned properties to advanced hardware design. Two sEMG sensors are used to detect the muscular activity of an amputee's stump, i.e., the muscular contractions of the forearm flexor and extensor muscles, which permit the closure and opening of the device, respectively, and its control. The two sEMG sensors were placed inside the socket and interface with the Hannes hand by means of dedicated conditioning and control electronics modules embedded within the "EMG processing board" shown in Fig. 1A, which was custom designed and returned the control signal to be sent to the "motor control board" module. The Hannes system is powered by a battery pack that is also placed inside the socket and is designed to last up to 1 day. Last, a magnetic plug connector is used to recharge the batteries when the system is not in use. The used controller is proportional; i.e., it sends velocity references to the hand

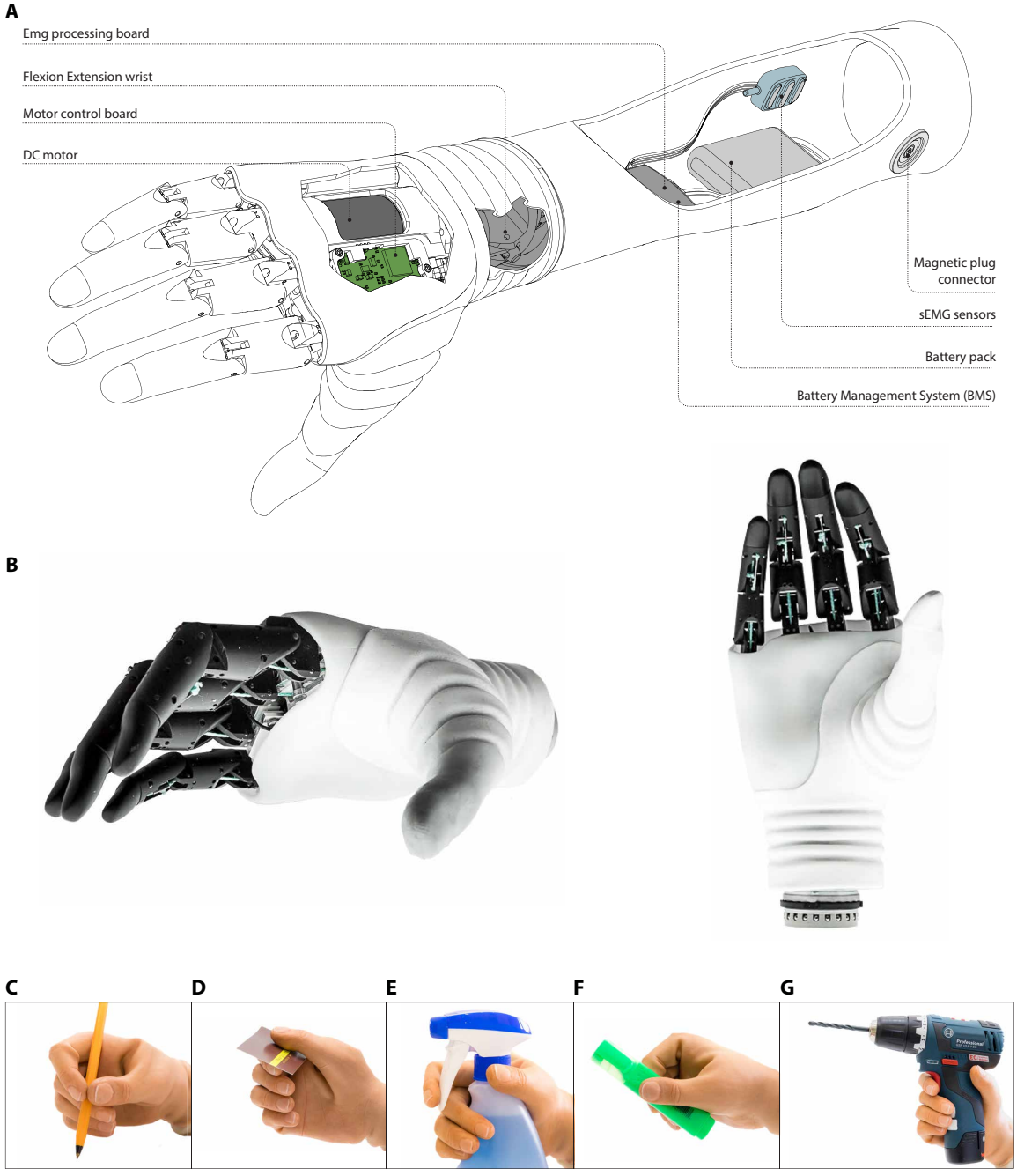

Fig. 1. Hannes system. It is composed of three main components, i.e., a myoelectric poly-articulated prosthetic hand, a passive F/E wrist module, and a myoelectric interface/controller. (**A**) Architecture: The DC motor and the motor control board are embedded within the myoelectric hand, whereas the sEMG-based myoelectric interface/controller is housed within the socket. The F/E wrist is placed between these two modules. (**B**) Views of the Hannes hand without glove. (**C** to **G**) Gloved device performing ADLs: (C) a precision grasp of a pen, (D) a lateral grasp of a business card, (E) a power grasp of a compliant object, (F) a lateral grasp of a marker, and (G) a power grasp of a tool.

that increase proportionally with the muscular activation. The control parameters are tuned for each person to achieve fine motion and force control of the device on each patient.

Experimental evaluation

The results from the experimental evaluation presented in this section validate that Hannes is able to satisfy the requirements mentioned earlier. Although anthropomorphism is assumed by design, as shown previously, the biomimetic performance and human-like grasping behavior were assessed experimentally.

Biomimetic performance superior to that required by ADLs

Force and velocity experiments were carried out to determine Hannes's performances in regulating the grasp through EMG control. The force capabilities of Hannes are reported in Fig. 4A. It can be observed that the prosthesis starts moving as soon as the EMG closure

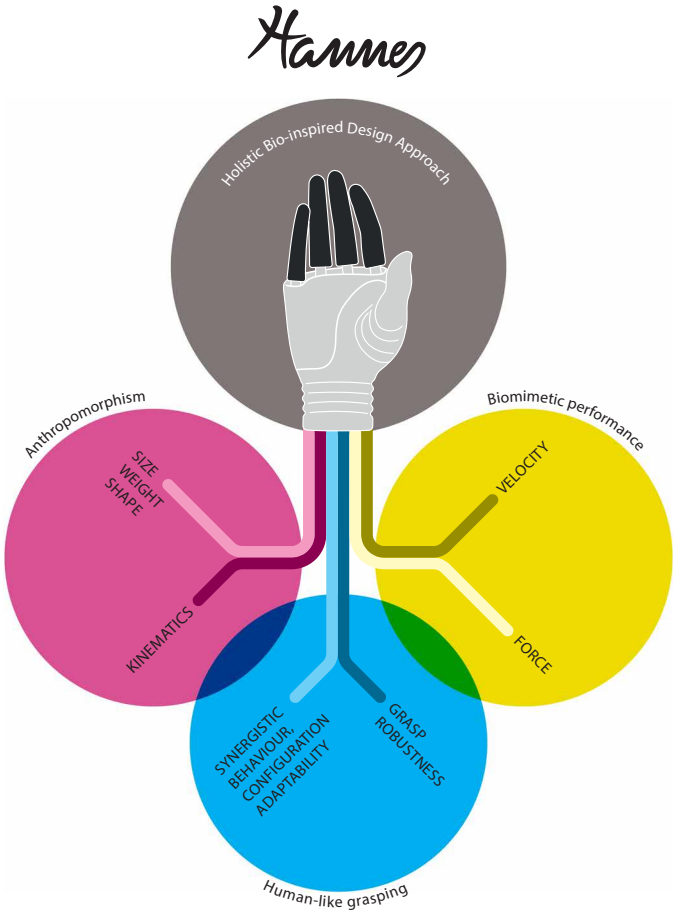

Fig. 2. The holistic biomimetic prosthesis design approach. The Hannes system was conceived using a holistic design approach that takes into account all the main characteristics which express anthropomorphism, human-like grasping, and biomimetic performance since its early development stage. These key biomimetic factors complementarily converge and have all been incorporated into the Hannes system.

threshold is reached. The digits of Hannes then enter into contact with the hand dynamometer, and the force starts increasing. The first experiment, shown in Fig. 4A (left), demonstrates that the force can be modulated to slowly increase and decrease by means of the user through an appropriate regulation of the EMG activity. The second experiment, shown in Fig. 4A (right), shows that when rampant EMG activation is applied, the prosthesis can quickly close and reach the peak force of about 150 N in less than 0.25 s.

The angular velocities of Hannes's joints for a full-speed closure are shown in the plot in Fig. 4B. The plot shows that the MCP joints reach a peak velocity of about 4 rad/s (229°/s), whereas the proximal IP (PIP) joints can reach a peak velocity of about half this value. Hannes can perform a full closure in less than 1 s.

Human-like synergistic behavior

Kinematic analysis was conducted to determine the extent to which the Hannes hand exhibits human-like synergistic kinematic behavior. The other aspect related to human-like grasping, i.e., grasp robustness, was evaluated empirically through observation; the result is demonstrated in Movie 2.

Figure 5 (C and D) shows the pairwise Pearson correlations of the joint angles of Hannes and the human hand, respectively, during

Movie 1. Summary of Hannes hand.

the grasping of the objects in Fig. 5 (A and B). The analysis of the human hand postures revealed correlations ($r > 0.8$, $P < 0.01$) between (i) the MCP flexions of adjacent fingers and (ii) the abduction of neighboring fingers, with the exception of the little finger. These results are consistent with data in the literature (*23*, *47*, *48*).

The correlation matrix of Hannes exhibited the same correlations as those observed for the human hand ($r > 0.8$, $P < 0.01$): (i) MCP flexions and (ii) MCP abductions of the neighboring fingers. The finger-adjacency effect observed for the human hand is even more evident for Hannes, showing large correlations even for the index-little pair. Furthermore, the PIP and DIP joints exhibit correlations within each finger and with the immediate neighbor ($r > 0.80$, $P < 0.01$). The observed correlations among the joints of Hannes suggest that there is possibility of a dimensionality reduction of the postures of Hannes. We therefore conducted PCA.

Figure 5E shows a comparison of the variance for each component (up to the eighth component) for Hannes and the human hand. PCA revealed that the first synergy of the human postures accounts for about 39% of the total variance of the system, 23% in PC2 and 14% in PC3 (Fig. 5E). In cumulative terms, the first two PCs accounted for 62% of the variance of the data, whereas we observed that the explained variances are 76 and 87% for the third and fifth components, respectively. These results are consistent with (*23*, *47*).

In Hannes, the first synergy is much more predominant than in the human hand, accounting for about 75% of the variance, whereas the second synergy decreases markedly to about 12%. In cumulative terms, the first two PCs account for about 86% of the variance of the data. Including up to the third and fifth components, the cumulative values reach 97 and 99%, respectively.

We briefly describe the postures corresponding to each synergy in Hannes:

1) PC1 corresponds to an opening closure of the hand, mainly by means of finger MCP flexion combined with a little thumb rotation and abduction.

2) PC2 is responsible for the PIP F/E of the fingers. Thumb abduction is also observed.

3) PC3 corresponds to thumb rotation and thumb abduction.

The obtained results for the first synergy (PC1) obtained for Hannes are consistent with previous research on the human hand (*23*, *47*). Although to a lesser extent, the second and third PCs also appear to contribute to the same DOFs typically involved in human

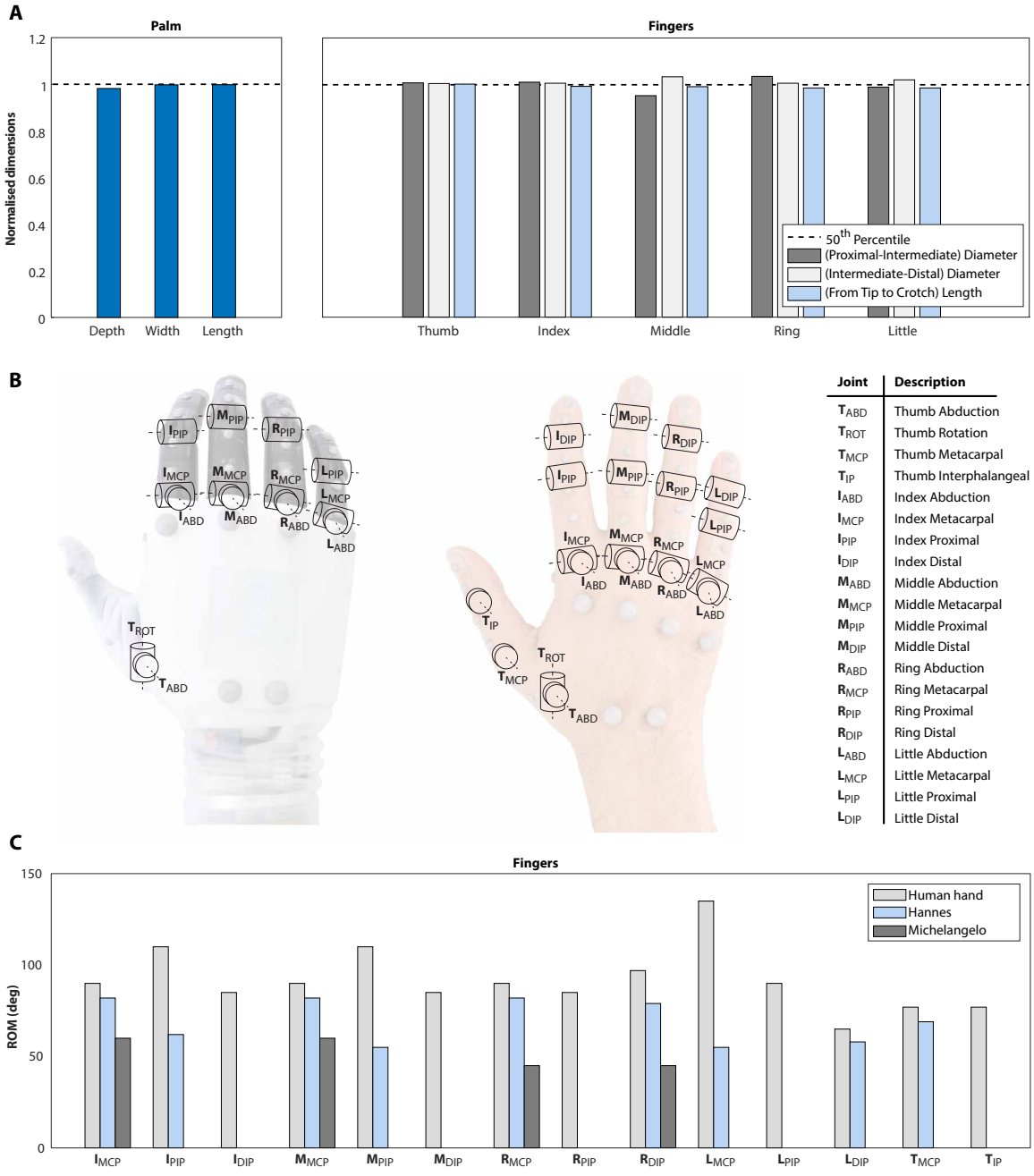

Fig. 3. Anthropometry of Hannes. The high fidelity in the reproduction of biomimetic anthropomorphism in Hannes is shown by directly comparing the size, shape, and kinematic model of Hannes with anthropometric data and kinematics of a typical human hand and the Michelangelo prosthesis that is used as a gold standard. (**A**) Dimensions of Hannes and a comparison with the 50th percentile human hand; in addition, refer to table S1. (**B**) Kinematic model and nomenclature of Hannes and the human hand. (**C**) ROM of the 50th percentile human hand, Hannes, and Michelangelo prosthesis.

synergies for grasping tasks, with the exception of the thumb movements in PC2 (*23*); see also Movie 3 and fig. S1. To analyze the first two PCs in detail, Fig. 5 (F and G) presents how these PCs combine to form different postures for grasping the nine objects in the trials. These postures can be determined by the points that identify each single object, displayed in the plane formed by PC1 and PC2. Figure 5 (F and G) shows that the MCP finger joints are completely extended at PC1min, whereas the fingers fully flex at the rightmost point, which confirms the discussion above for PC1; see also Movie 3 and fig. S1. Analyzing PC2 for the human hand, the PIP joints are extended at PC2max, while they progressively flex toward PC2min. In Hannes's second synergy, there is also a predominant effect on the PIP joints, although the motion is reversed, i.e., from extension at PC2min to flexion at PC2max. Analyzing the thumb, instead, there is a rotation component in the human hand that is not present in Hannes. Although there are differences between the PCs computed for the human hand and Hannes, the plots in Fig. 5 (F and G) clearly show that the objects are mostly distributed on the PC1 axis for Hannes, in contrast to the

case for the human hand. Last, the motion of the DIP joints in our human data for both PC1 and PC2 is very small, which has been confirmed by previous studies (*47*, *49*) and validates our design choice of keeping them locked.

Pilot clinical trials show the high potential of Hannes

The evaluation was conducted on three participants by executing tests and using questionnaires that are specifically meant to measure prosthesis use ability. Table S2 provides the obtained scores for the three participants with the reference hand during the baseline assessment (TB) and with the Hannes system during the study (T0, T1, and T2); see Materials and Methods for details. Figure 6 also summarizes the improvement/deterioration in the tests and questionnaires scores from the baseline to the end of the study by reporting the difference between the scores recorded at T2 and the scores recorded at TB.

The results obtained with the Minnesota Manual Dexterity Test, Placing only (MMDT-P), which measures the time required to move a set of objects, were, on average, better with Hannes than with the reference prosthesis. Participants #1 and #2 performed better with Hannes, with decreases in the time needed to perform the task of about 10 and 30%, respectively, whereas participant #3 performed better with the reference hand: The timings obtained during T0, T1, and T2 were longer than those obtained during TB, although there was a marginal increase of about 15% as shown in Fig. 6 (note that for the Minnesota test, negative values indicate an improvement and positive values indicate deterioration). This result can be explained by the fact that, with respect to other participants, participant #3 only had experience with a tridigital hand and was not familiar with a poly-articulated hand. In detail, although the tridigital hand was already represented into his body schema (*50*), the ring and little fingers of Hannes were not: Two weeks of training are insufficient to shape neural plasticity so as to incorporate a poly-articulated prosthesis into body representation (*51*). Participant #1 performed better with Hannes from the beginning of the experimental procedure (M ± SD: 132 ± 6 s at T0 versus 137.33 ± 15.31 at TB; table S2), possibly because the participant was an expert user of a poly-articulated hand and thus did not experience difficulty in adapting to Hannes's grasp. However, despite the initial performance, all participants improved their results on the Minnesota test with Hannes during the training (from T0 to T2; see table S2). Similar results were obtained for the Southampton Hand Assessment Procedure (SHAP) test: The scores obtained at TB and T2 were comparable across the participants, and in many cases, there was an increase from TB to T2 (see the positive values in Fig. 6). The results from this test for participant #1 were overall more neutral, probably because this participant was already an expert user of poly-articulated hands. Critical results were only obtained for the lateral grasp with participants #1 and #3 due to a technical issue experienced during the whole execution of the trial that did not allow a firm grasp in this configuration. This was due to suboptimal mechanical fitting between the pin and the hole of the thumb's MCP joint that caused high friction that resulted in poor thumb performance. This problem was solved in the device after the trials with a minor mechanical

Movie 2. Amputated participant using Hannes.

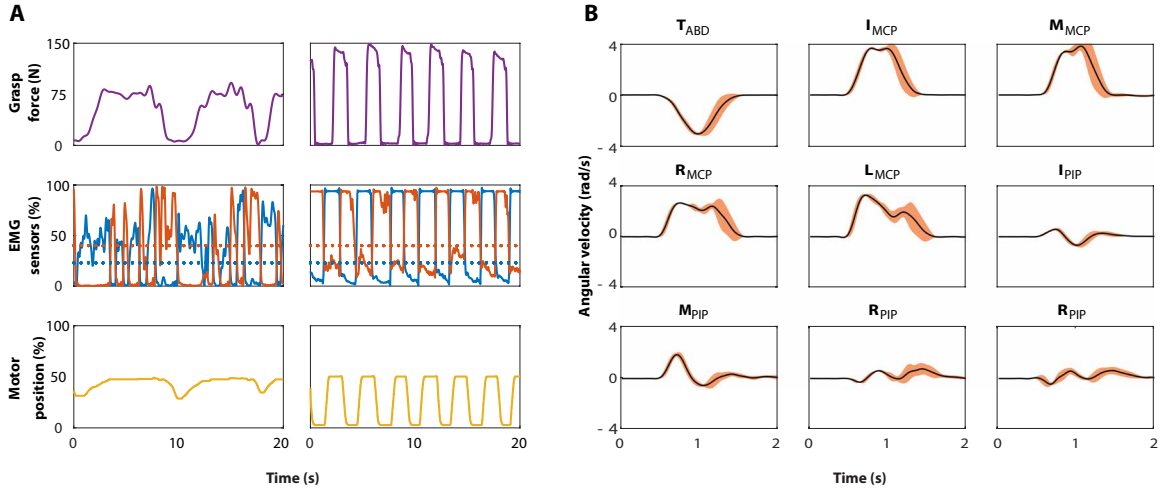

Fig. 4. Force and velocity experiments. Direct evaluation of the force and velocity capabilities of Hannes and the controllability of the force regulation. (**A**) Regulation of the force (left) and power grasps (right) regulated through direct EMG control. In the EMG plots, the red lines indicate opening EMG sensor activity, and the blue lines indicate closure EMG sensor activity. The red and blue dotted lines indicate the activation thresholds for opening and closure EMG sensor activities, respectively. In the bottom plot, the normalized motor position ranges from 0 to 100% and denotes motor positions that correspond to fully open and fully closed hand, respectively. In this test, the grasp occurs at about half the motor travel, i.e., when the motor position assumes a value of around 50%. (**B**) Angular velocities of the main articulation of Hannes during a full-speed closure. The black lines indicate the median values. The shaded areas indicate the SD.

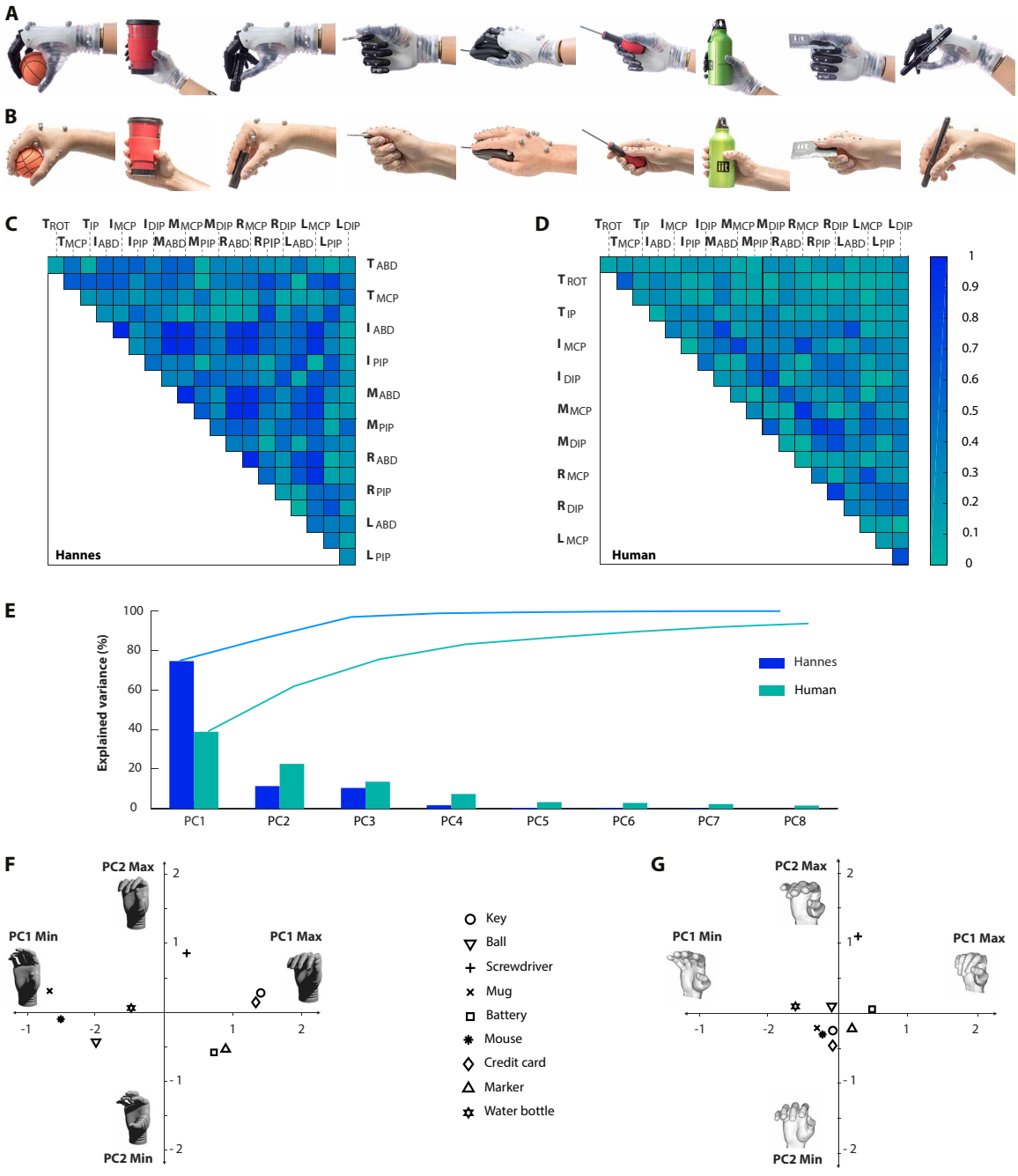

Fig. 5. Kinematic analysis of Hannes and its synergistic behavior. Static and dynamic kinematic behavior of Hannes and its resemblance to that of the human hand by direct comparison of postures, correlation patterns, and synergies, and their combination while grasping the different objects. (**A** and **B**) The static postures of Hannes and the human hand, respectively, for each grasped object. Patterns of correlation in the joint angles during the grasping of nine objects are shown in (**C**) for Hannes and in (**D**) for the human hand. (**E**) Comparison of the Pareto plot of the variances for each PC (up to the eighth). (**F**) Scatter plot of the Hannes postures projected along PC1 and PC2. (**G**) Scatter plot of the human hand postures projected along PC1 and PC2. The markers indicate the median position of the three participants ((*73*) credited for the hand and mesh models of the human). The 3D views of the postures of Hannes and the human hand on the right and left in (F) and (G), aligned with the horizontal axis, are the postures with minimum and maximum values of PC1. The top and bottom postures, aligned with the vertical axis, correspond to the maximum and minimum values of PC2, respectively.

fix. The execution of these tests by amputated participants and the correct accomplishment of lateral and precision grasps by the Hannes hand can be observed in movies S1 and S2, respectively. Please note that the grasps shown in movie S2 are performed by a healthy participant.

Beyond these tests, the questionnaires provide a qualitative evaluation of the independence of the user in the execution of ADLs. Specifically, the Orthotics and Prosthetics User Survey Upper Extremity Functional Status (OPUS-UEFS) questionnaire measures functional activities executed by amputees with a prosthesis. As reported in

Fig. 6, for participant #1, the reference hand enabled higher scores and therefore seemed more desirable, according to this questionnaire. Participant #2 showed an improvement with the use of Hannes, whereas participant #3 improved their scores with Hannes with respect to the scores achieved with the reference hand.

The Disabilities of the Arm, Shoulder, and Hand (DASH) questionnaire returns measurements of the level of impairment in functional activities of the upper limb with scores ranging from 0 (functional activity like in a natural hand) to 100% (no function at all). According to this questionnaire (Fig. 6 and table S2), participants #1 and #2 performed better with the reference prosthesis (scored with 0), whereas for participant #3, the level of functionality was unchanged. The change in the DASH scores cannot be represented as a percentage; thus, in Fig. 6, we report the difference between the scores at T2 and TB (note that for the DASH, negative values indicate an improvement and positive values deterioration).

The Trinity Amputation and Prosthesis Experience Scales (TAPES) questionnaire, which considers the degree of satisfaction in the utilization of a prosthesis, promotes the Hannes system over the reference hand in the case of participants #2 and #3, as the scores improve by three and five points, respectively (Fig. 6), whereas participant #1 achieves a slightly higher score with the reference prosthesis (Fig. 6 and table S2). Last, according to the final evaluation questionnaire (table S3), participants #1 and #2 greatly appreciated Hannes.

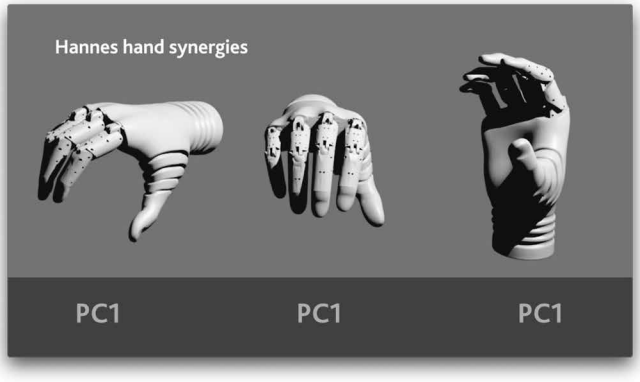

Movie 3. Principal components analysis.

DISCUSSION

An analysis of the anthropomorphism of Hannes showed that the vast majority of the dimensions are reproduced with high fidelity, in addition to the kinematics, which replicate most of the DOFs (Fig. 3, A and B). An exception is the approximation in the design for the fixation of the digits' distal DOFs. However, when compared with other hand joints, the DIP joint contributes minimally to the functionality of the hand. By extracting the data in (*47*), it can be simply demonstrated that this joint, considering the first three synergies, among the five fingers, has an average ROM that is about four times smaller than that of the other DOFs. The smaller significance of this DOF means that it is appropriate to keep the DIP locked and does not undermine biomimicry and effectiveness. In addition, Hannes exhibits MCP ROMs that are very similar to those of a human hand in most digits; this difference is higher for the PIP joints. Provided that grasping tasks are involved, this kinematic discrepancy does not represent a problem, because the maximum flexions measured for these DOFs in the range of the objects tested are smaller than the mentioned ROMs: The maximum measured I_{PIP}, M_{PIP}, R_{PIP}, and L_{PIP} flexions across all the participants and grasped objects are 51.9°, 47.1°, 39.8°, and 44.2°, respectively, which are smaller than the available ROMs reported in Fig. 3C. This result provides evidence that Hannes has exceptionally high levels of anthropomorphism, even when compared with state-of-the-art devices, such as the Michelangelo prosthesis. Last, the mass of the device is 480 g, which is close to that of its biological counterpart (*52*). Note that a prosthesis weight that matches the weight of a human hand is generally described by users as being too heavy, and it is well known that the perceived weight increases due to the fact that the weight is borne by the stump's soft tissue and not the skeletal system as in the case of healthy participants (*53*). Nevertheless, it is extremely challenging to replicate weight levels below the weight of a human hand because of the constraints of current electromechanical systems and

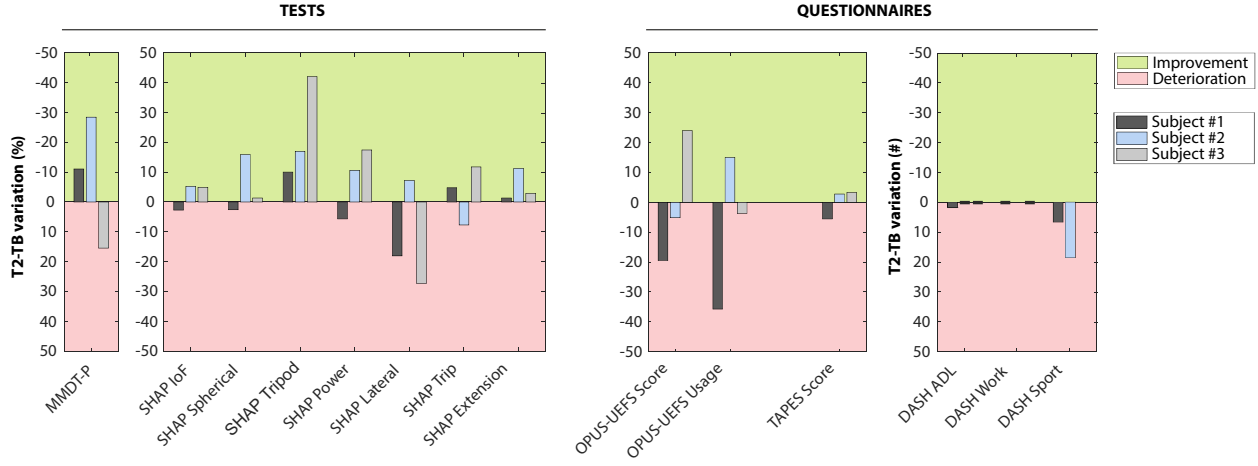

Fig. 6. Rate of improvement of the scores for the tests and questionnaires. The differences between the scores at T2 and TB are reported for each participant in histogram format for a direct visualization of the rates of improvement. These rates—for the MMDT-P and SHAP tests (**left**), and the OPUS-UEFS, TAPES, and DASH questionnaires (**right**)—are reported. The difference is indicated as the percentage variation for all the tests and questionnaires except for DASH; the improvement/deterioration is indicated by the T2-TB negative/positive values for the MMDT-P and the DASH and T2-TB positive/negative values in other cases.

material technologies. Hence, we decided to set the reference weight value to the weight of a human hand.

Hannes is also very biomimetic in terms of performance: Its mechatronic design is such that its performance is very close to that exhibited by a human hand. The results show that the device outperforms the velocity levels and grasping forces needed for the execution of ADLs. The user can modulate the force when grasping an object, which is necessary for dexterity and grasp robustness (*11*, *12*). In addition, the delay between a muscle contraction and a hand actuation is about 10 ms, which is smaller than the physiological electromechanical delay (*54*) and cannot be perceived by the user. This feature, combined with the high motion speed achieved by Hannes, is fundamental for the desired high effectiveness of the prosthesis (*5*, *10*) and crucial for achieving embodiment of the device (*19*). To the best of the authors' knowledge, the levels of force achieved by Hannes are superior to those of most existing research and commercial poly-articulated devices, with the exception of the lateral grasp of the Michelangelo prosthesis (table S4). Few prostheses can achieve higher speeds—for example, (*34*, *44*)—but only at the expense of force, which is often much smaller than the reference ADL level (*5*). From the performance perspective, the key property of the presented design, as compared with other existing designs, relies on the concurrent achievement of high scores in weight, force, and velocity levels (table S4), as well as highly anthropomorphic shape, size, and kinematics and highly robust grasping capabilities (Movie 1). To achieve the final goal, however, the aforementioned features must be combined with highly biomimetic synergistic behavior, as discussed next.

PCA was conducted on both the human hand and Hannes for direct comparison. The correlation matrix in Fig. 5C shows that Hannes exhibited a similar correlation pattern to the human hand. Although the correlation coefficients tend to be larger for Hannes, which is expected from an underactuated system with moderate intertrial variability, for both the human hand and Hannes, adjacent fingers have a higher correlation than nonadjacent fingers (*23*, *48*). This effect is even more relevant in Hannes than the human hand for two main reasons: Due to the one-DOF underactuation of all fingers, the kinematics in Hannes are expected to be more correlated than in the human hand, and the ergonomics of daily life objects leads to postures in which adjacent fingers tend to have a similar orientations and attitudes. Overall, Fig. 5 (C and D) shows similarity in the patterns obtained by the human hand and Hannes, particularly in the correlation between neighboring MCP joints (all with $P < 0.01$). These considerations have clear reflections on the resulting coefficients of the first human hand PC, which is consistent with the literature (*23*, *55*). For Hannes, the related PC1 behavior is very close to that of the human hand, and the first synergy exhibits a marked predominance of the variance over the other synergies, more than that found for the human hand, where the variance is more evenly distributed as observed in (*23*). We expect that this effect might be reduced in designs that can independently reproduce more synergies. This could be obtained by including further degrees of actuation, which would lead to a reduction of PC1 variance with consequent increase in the variance score of higher order PCs. Yet, although Hannes was designed to implement the first human synergy with high fidelity, other PCs were obtained. These PCs represent a "side effect" that results from the mechanical intrinsic ability of Hannes to adapt to the shape of the grasped object, which imposes the final configuration of the device and contributes to the human likeness of Hannes's posture. Although PC2 and PC3 observed for the human hand and Hannes are responsible for moving the same set of joint angles, with the exception of the thumb motion in PC2, there are differences in their respective patterns. However, this is not an issue, because previous studies demonstrated that, in a human hand, only the first synergy requires an assumption of repeatable behavior, whereas the trends of higher-order synergies can substantially vary depending on the boundary conditions (*56*). In this study, these differences are mainly caused by imperfections in the kinematic model of Hannes, which is clearly not identical to that of a human hand, particularly in terms of the thumb and the idiosyncrasies among the participants' hands (*57*). Furthermore, PC2 and PC3 for Hannes assume plausible biomimetic behavior. Hence, these results provide key evidence for the exceptional biomimicry of the grasping postures of Hannes and demonstrate its ability to reproduce synergistic human-like grasping behavior. Attempts to reproduce such a characteristic in prosthetic hands were made in (*25*); however, because the kinematics of that device roughly approximated that of a human hand, the resulting behavior could not be compared with that of a human hand. This issue was overcome in (*35*); however, the performance levels were well below the required biomimetic force and speed values. In contrast, Hannes exhibits high levels of biomimicry during grasping, as shown in Fig. 1 (C1 to C5), Movies 1 and 2, and movie S1. Furthermore, the presented approach based on direct hardware implementation of PCs strongly facilitates the implementation of biomimetic control: The high human likeness achieved in this work is realized using a simple direct proportional control. This means that evolutions of this design, which will include the capability of reproducing more PCs—through, e.g., the implementation of more degrees of actuation—will pave the way to strategies that can seamlessly and optimally exploit the potential offered by the proposed hardware approach. Promising control approaches in this perspective are methods based on postural/abstract control, which combine different PCs during motion in a flexible and biomimetic way and therefore enhance the controllability of the device (*58*–*63*).

Hannes's results in the pilot clinical trials were, on average, higher than those for advanced state-of-the-art devices. Hannes provided high and seamless configuration adaptability during both grasping and manipulation, offering high grasp stability and robustness (*11*, *43*). The high scores obtained in the tests suggest that Hannes has a quick learning curve; hence, much better results are expected with a refined version of the device and appropriate experience and training to allow the amputees to develop suitable grasp strategies. As expected, in most of the tests and questionnaires, the amount of improvement from TB to T2 was stronger in participants that normally use a tridigital hand (i.e., participants #2 and #3), although the improvements were achieved at the expense of slower learning rates than the learning rate of participant #1. Participants #2 and #3 had to learn the different behaviors of the poly-articulated hand; participant #2 obtained higher scores than participant #3, which can be explained possibly because the participant was younger and by the fact that the participant occasionally used poly-articulated hands. The role of training and practice is described in literature as a critically important factor for establishing the embodiment of a prosthetic device in terms of its representation into the user's body schema after use-related changes in brain plasticity (*64*). Last, note that the lateral grip test was the only test that demonstrated poor performance because of a technical problem that was solved after the trials were completed, as explained in Results. Movie S2 demonstrates the capability of the fully functional Hannes hand to perform lateral and

precision grasps. Please note that the grasps shown in this video are performed by healthy participants. Participants #1 and #3 had poor scores with Hannes, whereas participant #2 had marginally better scores.

The questionnaire scores were, on average, comparable with those obtained with the reference prosthesis. Although such results appear to be not as promising as those obtained for the tests, the three participants verbally confirmed that they truly appreciated the high resemblance of Hannes with a human hand in terms of human-like behavior and anthropomorphism, as shown in Movies 1 and 2 and movie S1. In addition, the participants were very satisfied with the usability, overall effectiveness, and robustness during the trials. This was confirmed by the results of the final evaluation questionnaires, which had high scores for two out of three participants (tables S2 and S3). The contradiction between the positive direct user feedback and the average questionnaire scores can be explained by the fact that questionnaires focus on effectiveness in the execution of everyday activities and assume that the participant has become familiar with the device by developing appropriate grasping strategies. This familiarity requires consistent training and use that can only be achieved with more time than the time allowed in this study: 16 days. Much better results are therefore expected with longer training times. In contrast, the test results showed that the potential of the device to effectively execute grasping tasks is very high, apart from the aforementioned lateral grip issue; in addition, considering the relatively short training time, the scores are promising and show the very high potential of Hannes.

One of the main limitations of this study is that the Hannes system has been tested on a small number of participants. However, the participant sample is representative of the potential end-users because it includes young and elderly individuals with different years of myoelectric hand experience. Furthermore, the main drawback of the extreme exploitation of the underactuation concept used in this work is that it lacks versatility when different grasps styles are required by the participant. Again, this might be overcome by incorporating additional actuators to the current design, which can support the execution of different PCs.

We conclude by stating that one of the paramount concepts to be considered in the design of prosthetics is that prostheses must promote true embodiment so that they can actually be perceived as part of the body rather than a "simple" tool. We believe this feat can only be achieved by means of a firm concurrent incorporation of the discussed key biomimetic properties, particularly grasp force, velocity, robustness, anthropomorphism, and static and dynamic biomimicry (*5*, *30*), Movie 1, which may lead to realizing the ultimate and most fundamental goal of upper limb prosthetics: increasing the rate of acceptance.

MATERIALS AND METHODS

The goal of this research was to develop and evaluate a prosthetic hand that could achieve the three main design goals addressed in Fig. 2. Biomimetic levels of force, velocity, and weight are possible because of appropriate component sizing and a highly integrated and efficient centralized design that uses one motor to drive all the articulations of the hand implemented into a highly anthropomorphic shape. Human-like grasping properties—such as robustness, stability (*5*, *11*, *43*), and synergistic coordination of the fingers (*17*, *18*, *22*)—are implemented via an underactuated differential drive mechanism, which implements simultaneous synergistic kinematic behavior, configuration adaptability, and robust grasping through a combination of movement coordination and a uniform force distribution, as inspired by (*25*). The detailed mechanical model of Hannes is reported in the Supplementary Materials.

The evaluation of the mentioned static and dynamic biomimetic properties have been evaluated by means of lab tests that included the use of motion capture systems and force sensors for the measurement of velocity and kinematic behavior and grasp forces, respectively. In addition, the obtained kinematic data were also used for PCA on both the human hand and Hannes.

A pilot clinical trial was performed with the primary goal of defining Hannes's functionality, safety, and reliability and assessing the potential benefits regarding the quality of life of amputees. Three amputated participants could autonomously use Hannes at home to perform ADLs for a period of about 2 weeks. Tests and questionnaires were used before and after this phase.

Hannes's mechatronics

Poly-articulated prosthetic hand

Hannes's palm houses the main components of the hand—an electric actuator, a control board, sensors, and the transmission mechanism—whereas the F/E extension flexible wrist is located at the base of the device. The power train consists of a compact, high-power-density DC motor coupled to a custom-made hypocycloid gearbox. A 3D view of the assembly is shown in Fig. 7A. The power train actuates the leader wire, thus transmitting the force F_A and speed to the cable-based mechanism housed in the palm. The leader wire originates from the motor and ends in the thumb, passing through two differential elements mounted onto linear guides that are each made of a custom-made bush bearing and two rails along which the bushing moves. Each bushing houses two idle pulleys: one pulley supports the leader wire, whereas the second pulley is used by the follower wire to actuate two adjacent fingers. There are two follower wires: The first wire moves the index and middle fingers, while the second follower wire is used to actuate the ring and little fingers. To avoid slack on the leader wire, springs acting on the linear guides are also included in the assembly.

Fingers

Figure 7B shows a finger and its kinematics. The mechanism relies on dowel pins to guide the wires in the fingers and to maximize the integration density and robustness, which additionally implements a biomechanically plausible hinge joint-based solution (*65*). Two wires are observed in the cross-sectional view: On the lower side of the figure, the follower wire comes from the corresponding linear guide and terminates on the distal phalanx, and the wire located at the top is used for the extension of the finger and is part of a mechanism that includes a compression spring of stiffness K^j_{ext}, where j = [1, 2, 3, 4] identifies the finger such that 1 corresponds to the index and 4 to the little. This component generates tension that increases with the flexion of the finger, and a pretensioning mechanism is located on the other end to set the appropriate preload. As the motor applies torque, the follower and return wires both get tensioned, which results in a compression of the extension spring. Hence, the tensioned return wire generates torque on the MCP and PIP joints that is an antagonist to the torque generated by the follower wire. Thus, the magnitude of the tension force applied to the return wire is proportional to F^j_A, with a factor that is easily computed

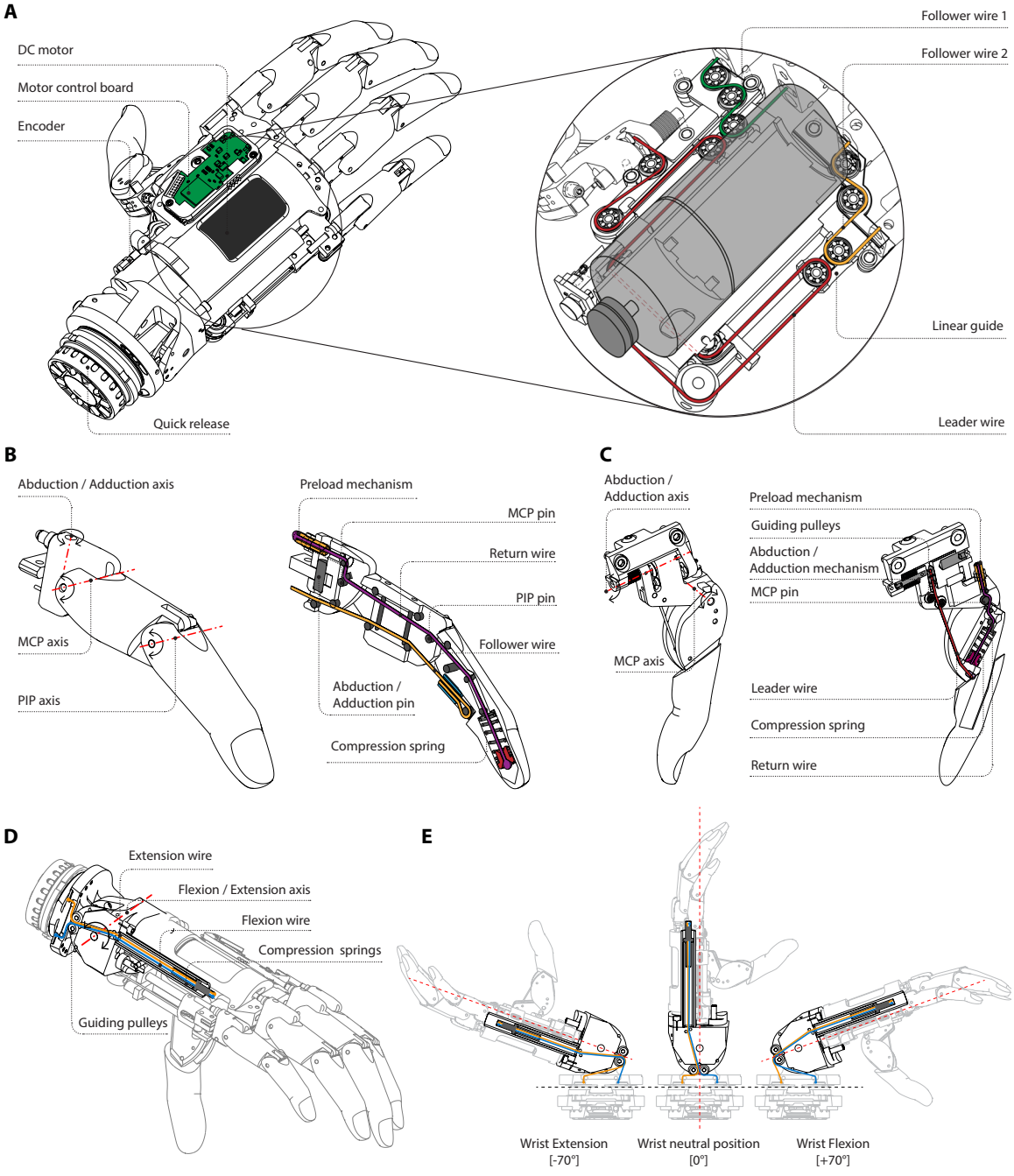

Fig. 7. Hannes's mechatronics. The core mechatronics of the Hannes hand in its components: palm, digits, and wrist. (**A**) 3D view of the hand (left) and cross section of the transmission mechanism located in the palm (right). The leader wire, follower wire 1 (index and middle fingers), and follower wire 2 (ring and little fingers) are shown in red, green, and yellow, respectively. (**B**) Finger kinematics (left) and mechanical design (right). (**C**) Thumb kinematics (left) and mechanical design (right). (**D**) Detailed cross section of the F/E wrist integrated in Hannes and (**E**) the F/E wrist in three configurations: (left) maximum extension, (middle) neutral position, and (right) maximum flexion.

by the ratio of the respective levers. When the motor unwinds the leader wire, the follower wire slackens, with a consequent extension of the return spring and finger. When the follower wire is tensioned with force F_A^j, fig. S4, two resulting lever arms act on the MCP and PIP joints, making it possible to set appropriate joint torques for these articulations. In particular, the MCP torque is designed to be about twice the torque of the PIP joint, which permits the regulation of the activation timing of each joint and a uniform force distribution along the finger to mimic the first human kinematic synergy.

Thumb

The thumb comprises an active abduction/adduction joint that operates similarly to the MCP joint of the fingers, whereas the IP and DIP joints are locked, as shown in Fig. 7C. In addition, the thumb rotation is implemented by a custom-made spring-based plunger mechanism, Fig. 7C, that can lock the finger in three equally spaced

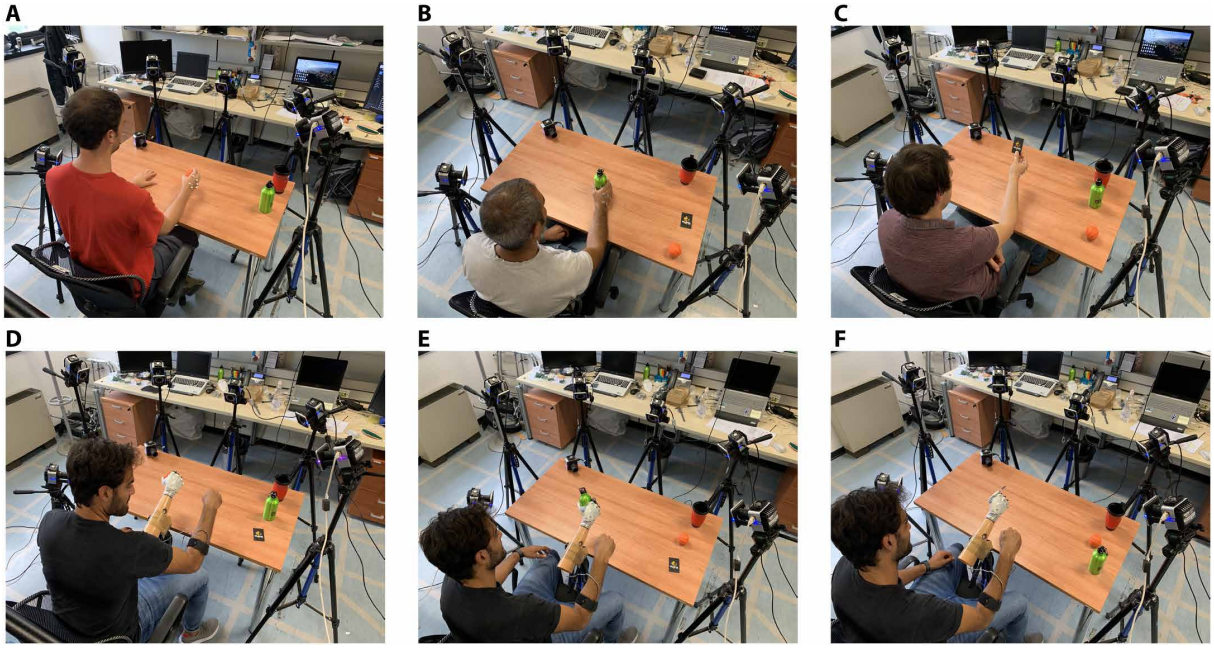

Fig. 8. Experimental setup of the motion capture analysis of Hannes and a human hand. Healthy participants and Hannes in the designed experimental setup performing grasps of objects of different size and shape. (**A** to **C**) Participants #1 to #3 grasping different objects, respectively. (**D** to **F**) Hannes grasping different objects. Hannes is controlled by the healthy participant using EMG control.

stable positions (fig. S2) to perform different grasp styles, as shown in Fig. 1 (C1 to C5), Movie 1, and movie S1. The closure timing of the thumb can be synchronized with the fingers by means of a screw-based mechanism that acts on the preload of the corresponding return wire, Fig. 7C. This is crucial to perform precision grasps correctly.

Passive F/E wrist module

The F/E wrist exploits a mechanical compression spring engaged by a cable-based system to reproduce elasticity. The wrist flexes and extends around a pin-based revolute joint (Fig. 7D). When the wrist is flexed, the flexion wire attached to the Hannes base at one end, and a compression spring at the other end is tensioned, compressing the elastic element and introducing slack to the extension wire; the opposite occurs when the wrist is extended (Fig. 7E). Both wires are based on Dyneema. The wires are guided by rectified pins along their paths and by two pulleys to preserve their integrity and guarantee high robustness for the entire system. Last, the proper preload of the spring avoids a backlash around the equilibrium position. In addition, a locking mechanism allows the wrist to lock in five equally spaced positions along an ROM similar to that of its biological counterpart, about ±70° (*46*). The exerted torque and stiffness values are also set to match those of the human hand (*66*): The maximum exerted torque is 0.75 Nm at the end of the stroke, which leads to an average stiffness of about 0.614 Nm/rad. A linear relationship exists between the rotation of the wrist and the compression of the spring, which is made possible by pins located along a profile defined by a circle with an axis located at the center of rotation. Thus, the torsional stiffness is quasi-linear.

Biomimetic performance experiments

Force

The prosthesis grasped a hand dynamometer that can measure the grasping force by means of a force sensor (Hand Dynamometer HD-BTA by Vernier). The motor position was regulated through direct EMG control to either regulate the prosthesis to move slowly and regulate the grasp force, as shown in Fig. 4A (left), or to perform power grasps with maximum speed to evaluate the maximum grasp force, as shown in Fig. 4A (left). The EMG sensors were two 13E200 MyoBock sensors made by Ottobock.

Velocity

Hannes was set up with the arrangement described in the following section to record the motion of each phalanx via a motion capture system. Hannes was controlled through an EMG interface to perform a full-speed closure, and no object was grasped in this experiment. The angles were recorded using the procedure described in text S2 and then postprocessed to obtain the angular velocities of each articulation through numerical differentiation.

Human-like synergistic behavior experiments

Participants

Three right-handed healthy participants (three males of 24 to 27 years with self-reported hand dominance) were tested. The same procedure was also conducted using a right-hand Hannes prosthesis through an able-bodied adapter. All participants were unaware of the purpose of the experiment and had no history of neurological or motor deficits.

Experimental setup

Six 850-nm VICON Vero V2.2 cameras (VICON Motion Systems, Oxford, United Kingdom; sampling frequency of 100 Hz, resolution of 2.2 megapixels, 330 frames per second) were used to record kinematic data from a set of passive reflective markers (MKR-4.0H and PM-9.5, B&L Engineering, California, USA) placed on participants' hands and Hannes, as shown in Fig. 8.

Procedure

The participants were instructed to sit on a chair with their forearm lying on a tripod to fix the initial position. First, a static acquisition was performed. Once the participants signaled that they were ready

to start a trial, they were asked to grasp one of the nine objects as they would consider most appropriate, hold the object for 1 s, and place the object back in its original position (Fig. 8, A to C). The procedure was repeated five times for each of the objects. The order in which the objects were grasped was randomized for each participant. Each participant was tested on different days at different times. The total duration of the experiment was about 1.5 hour per participant, with a break of a few minutes at the halfway point. The participants could choose to rest at the end of each trial. The same procedure was repeated using a right-hand Hannes prosthesis (Fig. 8, D to F). Hannes was placed in a fixed configuration by attaching the prosthesis to a stump locked to a fixed frame. The participant was asked to place an object within Hannes's reach so that the object could be grasped in a natural manner. Hannes was commanded to open/close using the EMG interface consisting of two EMG sensors mounted onto the right arm with an elastic band. The object was held for 1 s and then placed back in its original position by the participant. The procedure was designed to focus on the postures during grasping; reaching movements were not considered.

Principal components analysis

Correlation analysis was first conducted on the Hannes and human hand angle data to assess the extent to which the angular positions covaried with respect to each other, according to the kinematic model in Fig. 3B. PCA was then performed to obtain two full sets of postural synergies: one set for Hannes and one set for the human hand. The data were processed using the procedure explained in the "Angle extraction" section provided in the Supplementary Materials.

Pilot clinical trials

The clinical study was performed in collaboration with the Prosthetic Centre of INAIL (Istituto Nazionale per l'Assicurazione contro gli Infortuni sul Lavoro, Italian workers' compensation system) in Vigorso di Budrio (Italy). The testing procedures presented here were approved by the Ethics Committee of Bologna and Imola (CE-BI, protocol number 16051) in accordance with the guidelines of the Declaration of Helsinki.

Participants

Three male right-handed participants were enrolled (62, 29, and 55 years) with a transradial amputation of the right hand (the level of amputation was medial for participants #S1 and #S2 and distal for participant #S3) and no psychological comorbidity related to hand loss. All participants had residual muscles that were efficiently active and were expert in the use of a myoelectrically controlled hand [Ottobock Michelangelo (*38*) for participant #S1 and Ottobock Variplus (*67*) for participants #S2 and #S3].

Before their enrollment in the study, the participants signed an informed consent form. Table S5 summarizes the information about the recruited participants.

Experimental protocol

The participants were first tested (see the "Clinical evaluation measures" section) with their commonly used myoelectric prosthesis to assess their baseline (TB, see fig. S3). A myometric exam was then performed to evaluate the functional state of the residual muscles and the amount of EMG signals to establish the optimal positions of the Hannes EMG sensors.

After this phase, a training procedure followed (see table S6) during which participants became acquainted with the Hannes prosthetic system. Patients were then dismissed and provided with the Hannes prosthetic hand for a period of 16 days for domestic use and daily utilization.

The same tests used for baseline assessment were repeated with the Hannes hand before the training procedure (T0), at the end of the training period (T1), and at the end of the study (T2). Questionnaires (see the "Clinical evaluation measures" section) were presented at TB and T2.

Figure S3 depicts the experimental protocol and its various phases. The training consisted of a 4-hour procedure repeated for 4 days and involved accomplishing a set of tasks combining generic manipulation and the execution of several ADLs. Table S6 reports the executed tasks.

Clinical evaluation measures

The clinical evaluation consisted of monitoring parameters collected from the tests and questionnaires during different phases. We used two tests and four questionnaires. Specifically, the used tests were the MMDT-P and the SHAP. The first test assesses the ability to move small objects, and the score is the total number of seconds required to complete the chosen number of test trials (*68*). The second test measures the ability of the amputee in using a prosthetic hand, and the scores range from 0 to 100, where 100 corresponds to the typical functionality of a healthy limb (*69*) and are calculated for the overall hand function (index of function) or for specific postures (i.e., spherical, tripod, power, lateral, tip, and extension).

The questionnaires provide a qualitative evaluation of the independence of the user in the execution of ADLs. The used questionnaires were as follows:

1) the OPUS-UEFS module (*70*), which evaluates the efficacy in carrying out daily tasks, such as general self-care and the usage of domestic tools; the scores indicate how easily participants perform the tasks and if they use the prosthesis for these activities (a higher score indicates greater function);

2) the DASH questionnaire (*71*), which returns measurements of the functional activities of the upper limb in ADL, work, and sport and produces a score indicating the level of disability ranging from 0 (performance of a healthy limb) to 100 (full disability);

3) the TAPES questionnaire (*72*), which consider the degree of satisfaction in the utilization of the prosthesis in various tasks with scores ranging from 0 to 120; and

4) a final evaluation questionnaire (administered only at T2, see table S3).

The tests and questionnaires were used to assess the behavioral performance of the participants using a prosthetic hand and thus were performed both when participants used Hannes and the reference hand.

SUPPLEMENTARY MATERIALS

robotics.sciencemag.org/cgi/content/full/5/46/eabb0467/DC1

Text S1. Mechanical model
Text S2. Angle extraction
Fig. S1. First three synergies.
Fig. S2. The three stable rotation positions of the thumb.
Fig. S3. Outline of the experimental protocol.
Fig. S4. Forces acting in the palm mechanism.
Fig. S5. Mechanics of the digits.
Table S1. The main dimensions of the digits of the human hand and Hannes.
Table S2. Scores of the tests and questionnaires.
Table S3. Final evaluation questionnaire.
Table S4. Comparison table of commercial and research prosthetic hands.
Table S5. Participants' information.
Table S6. ADL tasks executed during the rehabilitative training with Hannes.

Movie S1. Amputees performing clinical tests with Hannes.
Movie S2. Healthy participants performing precision and lateral grasps with Hannes.
References (*74*–*76*)

REFERENCES AND NOTES

1. R. Vinet, Y. Lozac'h, N. Beaudry, G. Drouin, Design methodology for a multifunctional hand prosthesis. *J. Rehabil. Res. Dev.* **32**, 316–324 (1995).
2. C. Pylatiuk, A. Kargov, S. Schulz, Design and evaluation of a low-cost force feedback system for myoelectric prosthetic hands. *JPO J. Prosthet. Orthot.* **18**, 57–61 (2006).
3. H. Bouwsema, C. K. van der Sluis, R. M. Bongers, Learning to control opening and closing a myoelectric hand. *Arch. Phys. Med. Rehabil.* **91**, 1442–1446 (2010).
4. J. T. Belter, J. L. Segil, A. M. Dollar, R. F. Weir, Mechanical design and performance specifications of anthropomorphic prosthetic hands: A review. *JRRD.* **50**, 599–618 (2013).
5. R. F. Weir, in *Standard Handbook of Biomedical Engineering and Design* (McGraw-Hill, New York, USA, 2004), p. 32.1–32.61.
6. G. K. Patel, C. Castellini, J. M. Hahne, D. Farina, S. Dosen, A Classification Method for Myoelectric Control of Hand Prostheses Inspired by Muscle Coordination. *IEEE Trans. Neural Syst. Rehabil. Eng.* **26**, 1745–1755 (2018).
7. M. Zecca, S. Micera, M. C. Carrozza, P. Dario, Control of Multifunctional Prosthetic Hands by Processing the Electromyographic Signal. *Crit. Rev. Biomed. Eng.* **45**, 383–410 (2017).
8. E. A. Biddiss, T. T. Chau, Upper limb prosthesis use and abandonment: A survey of the last 25 years. *Prosthet. Orthot. Int.* **31**, 236–257 (2007).
9. C. Castellini, Chapter 19 - Upper limb active prosthetic systems – Overview, in *Wearable Robotics* (Elsevier, 2020), pp. 365–376.
10. H. A. Varol, S. A. Dalley, T. E. Wiste, M. Goldfarb, Biomimicry and the Design of Multigrasp Transradial Prostheses, in *The Human Hand as an Inspiration for Robot Hand Development*, R. Balasubramanian, V. J. Santos, Eds. (Springer International Publishing, Cham, 2014), vol. 95 of *Springer Tracts in Advanced Robotics*, pp. 431–451.
11. M. Controzzi, C. Cipriani, M. C. Carrozza, Design of Artificial Hands: A Review, in *The Human Hand as an Inspiration for Robot Hand Development*, R. Balasubramanian, V. J. Santos, Eds. (Springer International Publishing, Cham, 2014), vol. 95 of *Springer Tracts in Advanced Robotics*, pp. 219–246.
12. L. Biagiotti, F. Lotti, C. Melchiorri, G. Vassura, How Far Is the Human Hand? A Review on Anthropomorphic Robotic End-effectors (2004), pp. 1–21.
13. A. Bicchi, Hands for dexterous manipulation and robust grasping: A difficult road toward simplicity. *IEEE Trans. Robot. Automat.* **16**, 652–662 (2000).
14. C. Y. Brown, H. H. Asada, Inter-finger coordination and postural synergies in robot hands via mechanical implementation of principal components analysis, in *2007 IEEE/RSJ International Conference on Intelligent Robots and Systems* (IEEE, San Diego, CA, USA, 2007), pp. 2877–2882.
15. C. D. Murray, Embodiment and Prosthetics, in *Psychoprosthetics*, P. Gallagher, D. Desmond, M. MacLachlan, Eds. (Springer London, London, 2008), pp. 119–129.
16. E. J. Weiss, M. Flanders, Muscular and Postural Synergies of the Human Hand. *J. Neurophysiol.* **92**, 523–535 (2004).
17. A. Bicchi, M. Gabiccini, M. Santello, Modelling natural and artificial hands with synergies. *Phil. Trans. R. Soc. B.* **366**, 3153–3161 (2011).
18. A. Leo, G. Handjaras, M. Bianchi, H. Marino, M. Gabiccini, A. Guidi, E. P. Scilingo, P. Pietrini, A. Bicchi, M. Santello, E. Ricciardi, A synergy-based hand control is encoded in human motor cortical areas. *eLife* **5**, e13420 (2016).
19. F. de Vignemont, Embodiment, ownership and disownership. *Conscious. Cogn.* **20**, 82–93 (2011).
20. E. D'Anna, G. Valle, A. Mazzoni, I. Strauss, F. Iberite, J. Patton, F. M. Petrini, S. Raspopovic, G. Granata, R. D. Iorio, M. Controzzi, C. Cipriani, T. Stieglitz, P. M. Rossini, S. Micera, A closed-loop hand prosthesis with simultaneous intraneural tactile and position feedback. *Sci. Robot.* **4**, eaau8892 (2019).
21. A. M. Okamura, N. Smaby, M. R. Cutkosky, in *Proceedings 2000 ICRA. Millennium Conference. IEEE International Conference on Robotics and Automation. Symposia Proceedings (Cat. No.00CH37065)* (San Francisco, CA, USA, 2000), vol. 1, pp. 255–262.
22. M. Santello, M. Bianchi, M. Gabiccini, E. Ricciardi, G. Salvietti, D. Prattichizzo, M. Ernst, A. Moscatelli, H. Jörntell, A. M. L. Kappers, K. Kyriakopoulos, A. Albu-Schäffer, C. Castellini, A. Bicchi, Hand synergies: Integration of robotics and neuroscience for understanding the control of biological and artificial hands. *Phys. Life Rev.* **17**, 1–23 (2016).
23. M. Santello, M. Flanders, J. F. Soechting, Postural hand synergies for tool use. *J. Neurosci.* **18**, 10105–10115 (1998).
24. R. Gentner, J. Classen, Modular organization of finger movements by the human central nervous system. *Neuron* **52**, 731–742 (2006).
25. M. G. Catalano, G. Grioli, E. Farnioli, A. Serio, C. Piazza, A. Bicchi, Adaptive synergies for the design and control of the Pisa/IIT SoftHand. *Int. J. Robot. Res.* **33**, 768–782 (2014).
26. S. Li, X. Sheng, H. Liu, X. Zhu, Design of a myoelectric prosthetic hand implementing postural synergy mechanically. *Industrial Robot.* **41**, 447–455 (2014).
27. K. Xu, H. Liu, Y. Du, X. Zhu, Design of an underactuated anthropomorphic hand with mechanically implemented postural synergies. *Adv. Robot.* **28**, 1459–1474 (2014).
28. J. B. Rosmarin, H. H. Asada, Synergistic design of a humanoid hand with hybrid DC motor - SMA array actuators embedded in the palm, in *2008 IEEE International Conference on Robotics and Automation* (IEEE, Pasadena, CA, 2008), pp. 773–778.
29. M. C. Carrozza, G. Cappiello, S. Micera, B. B. Edin, L. Beccai, C. Cipriani, Design of a cybernetic hand for perception and action. *Biol. Cybern.* **95**, 629–644 (2006).
30. C. Cipriani, M. Controzzi, M. C. Carrozza, The SmartHand transradial prosthesis. *J. Neuroeng. Rehabil.* **8**, 29 (2011).
31. M. Grebenstein, A. Albu-Schäffer, T. Bahls, M. Chalon, O. Eiberger, W. Friedl, R. Gruber, S. Haddadin, U. Hagn, R. Haslinger, H. Höppner, S. Jörg, M. Nickl, A. Nothhelfer, F. Petit, J. Reill, N. Seitz, T. Wimböck, S. Wolf, T. Wüsthoff, G. Hirzinger, The DLR hand arm system, in *2011 IEEE International Conference on Robotics and Automation* (IEEE, Shanghai, China, 2011), pp. 3175–3182.
32. Y. Kurita, Y. Ono, A. Ikeda, T. Ogasawara, Human-sized anthropomorphic robot hand with detachable mechanism at the wrist. *Mech. Mach. Theory* **46**, 53–66 (2011).
33. E.-H. Kim, S.-W. Lee, Y.-K. Lee, A dexterous robot hand with a bio-mimetic mechanism. *Int. J. Precis. Eng. Manuf.* **12**, 227–235 (2011).
34. P. Slade, A. Akhtar, M. Nguyen, T. Bretl, Tact: Design and performance of an open-source, affordable, myoelectric prosthetic hand, in *2015 IEEE International Conference on Robotics and Automation (ICRA)* (IEEE, Seattle, WA, USA, 2015), pp. 6451–6456.
35. P. Weiner, J. Starke, F. Hundhausen, J. Beil, T. Asfour, The KIT Prosthetic Hand: Design and Control, in *2018 IEEE/RSJ International Conference on Intelligent Robots and Systems (IROS)* (IEEE, Madrid, 2018), pp. 3328–3334.
36. H. Ritter, R. Haschke, in *Humanoid Robotics and Neuroscience: Science, Engineering and Society*, G. Cheng, Ed. (CRC Press/Taylor & Francis, Boca Raton, FL, 2015), *Frontiers in Neuroengineering*.
37. S. J. Day, S. P. Riley, Utilising three-dimensional printing techniques when providing unique assistive devices: A case report. *Prosthet. Orthot. Int.* **42**, 45–49 (2018).
38. Ottobock, Michelangelo Prosthetic Hand (2020); https://shop.ottobock.us/Prosthetics/Upper-Limb-Prosthetics/Michelangelo-Axon-Bus-System/Michelangelo-Hand-AxonHook/Michelangelo-Hand/p/8E500~5L-M.
39. Ottobock, BeBionic Hand (2020); www.ottobockus.com/prosthetics/upper-limb-prosthetics/solution-overview/bebionic-hand/.
40. Ossür, iLimb Ultra (2019); www.ossur.com/prosthetic-solutions/products/touch-solutions/i-limb-ultra.
41. Vincent Systems, Vincent Hand, https://vincentsystems.de/en/prosthetics/vincent-evolution-3/.
42. K. Z. Zhuang, N. Sommer, V. Mendez, S. Aryan, E. Formento, E. D'Anna, F. Artoni, F. Petrini, G. Granata, G. Cannaviello, W. Raffoul, A. Billard, S. Micera, Shared human–robot proportional control of a dexterous myoelectric prosthesis. *Nat. Mach. Intell.* **1**, 400–411 (2019).
43. T. Laliberte, L. Birglen, C. M. Gosselin, Underactuation in robotic grasping hands. *Mach. Intell. Robot. Cont.* **4**, 1–11 (2002).
44. M. Controzzi, F. Clemente, D. Barone, A. Ghionzoli, C. Cipriani, The SSSA-MyHand: A Dexterous Lightweight Myoelectric Hand Prosthesis. *IEEE Trans. Neural Syst. Rehabil. Eng.* **25**, 459–468 (2017).
45. L. Resnik, S. L. Klinger, K. Etter, The DEKA Arm: Its features, functionality, and evolution during the Veterans Affairs Study to optimize the DEKA Arm. *Prosthet. Orthot. Int.* **38**, 492–504 (2014).
46. A. R. Tilley, H. D. Associates, *The Measure of Man and Woman: Human Factors in Design, Revised Edition, Wiley* (Wiley, New York, USA, 2001).
47. C. Della Santina, M. Bianchi, G. Averta, S. Ciotti, V. Arapi, S. Fani, E. Battaglia, M. G. Catalano, M. Santello, A. Bicchi, Postural hand synergies during environmental constraint exploitation. *Front. Neurorobot.* **11**, 41 (2017).
48. J. Lukos, C. Ansuini, M. Santello, Choice of contact points during multidigit grasping: Effect of predictability of object center of mass location. *J. Neurosci.* **27**, 3894–3903 (2007).
49. P. H. Thakur, A. J. Bastian, S. S. Hsiao, Multidigit movement synergies of the human hand in an unconstrained haptic exploration task. *J. Neurosci.* **28**, 1271–1281 (2008).
50. M. Pazzaglia, M. Molinari, The embodiment of assistive devices—from wheelchair to exoskeleton. *Phys. Life Rev.* **16**, 163–175 (2016).
51. F. Marini, C. F. Tagliabue, A. V. Sposito, A. Hernandez-Arieta, P. Brugger, N. Estévez, A. Maravita, Crossmodal representation of a functional robotic hand arises after extensive training in healthy participants. *Neuropsychologia* **53**, 178–186 (2014).
52. C. E. Clauser, J. T. McConville, J. W. Young, Weight, Volume, and Center of Mass Segments of the Human Body. *J. Occup. Environ. Med.* **13**, 270 (1971).
53. C. Pylatiuk, S. Schulz, L. Döderlein, Results of an Internet survey of myoelectric prosthetic hand users. *Prosthet. Orthot. Int.* **31**, 362–370 (2007).
54. P. R. Cavanagh, P. V. Komi, Electromechanical delay in human skeletal muscle under concentric and eccentric contractions. *Eur. J. Appl. Physiol. Occup. Physiol.* **42**, 159–163 (1979).

55. C. R. Mason, J. E. Gomez, T. J. Ebner, Hand synergies during reach-to-grasp. *J. Neurophysiol.* **86**, 2896–2910 (2001).
56. E. Todorov, Z. Ghahramani, Analysis of the synergies underlying complex hand manipulation, in *The 26th Annual International Conference of the IEEE Engineering in Medicine and Biology Society* (San Francisco, CA, 2004), vol. 2, pp. 4637–4640.
57. A. Naceri, A. Moscatelli, R. Haschke, H. Ritter, M. Santello, M. O. Ernst, Multidigit force control during unconstrained grasping in response to object perturbations. *J. Neurophysiol.* **117**, 2025–2036 (2017).
58. J. L. Segil, R. F. f. Weir, Design and validation of a morphing myoelectric hand posture controller based on principal component analysis of human grasping. *IEEE Trans. Neural Syst. Rehabil. Eng.* **22**, 249–257 (2014).
59. J. L. Segil, R. Kaliki, J. Uellendahl, R. F. f. Weir, A myoelectric postural control algorithm for persons with transradial amputations: A consideration of clinical readiness. *IEEE Robot. Automat. Mag.* **27**, 77–86 (2020).
60. T. Pistohl, C. Cipriani, A. Jackson, K. Nazarpour, Abstract and proportional myoelectric control for multi-fingered hand prostheses. *Ann. Biomed. Eng.* **41**, 2687–2698 (2013).
61. G. C. Matrone, C. Cipriani, E. L. Secco, G. Magenes, M. C. Carrozza, Principal components analysis based control of a multi-DoF underactuated prosthetic hand. *J. Neuroeng. Rehabil.* **7**, 16 (2010).
62. M. Dyson, J. Barnes, K. Nazarpour, Myoelectric control with abstract decoders. *J. Neural Eng.* **15**, 056003 (2018).
63. J. L. Segil, R. F. Weir, Novel postural control algorithm for control of multifunctional myoelectric prosthetic hands. *J. Rehabil. Res. Dev.* **52**, 449–466 (2015).
64. L. A. Wheaton, Neurorehabilitation in upper limb amputation: Understanding how neurophysiological changes can affect functional rehabilitation. *J. Neuroeng. Rehabil.* **14**, 41 (2017).
65. M. Grebenstein, M. Chalon, G. Hirzinger, R. Siegwart, Antagonistically driven finger design for the anthropomorphic DLR Hand Arm System, in *2010 10th IEEE-RAS International Conference on Humanoid Robots* (IEEE, Nashville, TN, USA, 2010), pp. 609–616.
66. D. Formica, S. K. Charles, L. Zollo, E. Guglielmelli, N. Hogan, H. I. Krebs, The passive stiffness of the wrist and forearm. *J. Neurophysiol.* **108**, 1158–1166 (2012).
67. Ottobock, MyoHand VariPlus Speed (2020); www.ottobock-export.com/en/prosthetics/products-from-a-to-z/arm-prosthetics/myohand-variplus-speed/.
68. J. Desrosiers, A. Rochette, R. Hébert, G. Bravo, The minnesota manual dexterity test: Reliability, validity and reference values studies with healthy elderly people. *Can. J. Occup. Ther.* **64**, 270–276 (1997).
69. C. M. Light, P. H. Chappell, P. J. Kyberd, Establishing a standardized clinical assessment tool of pathologic and prosthetic hand function: Normative data, reliability, and validity. *Arch. Phys. Med. Rehabil.* **83**, 776–783 (2002).
70. A. W. Heinemann, R. K. Bode, C. O'Reilly, Development and measurement properties of the Orthotics and Prosthetics Users' Survey (OPUS): A comprehensive set of clinical outcome instruments. *Prosthet. Orthot. Int.* **27**, 191–206 (2003).
71. P. L. Hudak, P. C. Amadio, C. Bombardier, D. Beaton, D. Cole, A. Davis, G. Hawker, J. N. Katz, M. Makela, R. G. Marx, L. Punnett, J. Wright, Development of an upper extremity outcome measure: The DASH (disabilities of the arm, shoulder, and head). *Am. J. Ind. Med.* **29**, 602–608 (1996).
72. P. Gallagher, M. MacLachlan, The Trinity amputation and prosthesis experience scales and quality of life in people with lower-limb amputation. *Arch. Phys. Med. Rehabil.* **85**, 730–736 (2004).
73. M. Schröder, T. Waltemate, J. Maycock, T. Röhlig, H. Ritter, M. Botsch, Design and evaluation of reduced marker layouts for hand motion capture. *Comput. Animat. Virt. W.* **29**, e1751 (2017).
74. S. B. Godfrey, K. D. Zhao, A. Theuer, M. G. Catalano, M. Bianchi, R. Breighner, D. Bhaskaran, R. Lennon, G. Grioli, M. Santello, A. Bicchi, K. Andrews, The SoftHand Pro: Functional evaluation of a novel, flexible, and robust myoelectric prosthesis. *PLOS ONE* **13**, e0205653 (2018).
75. Prensilia, Azzurra IH2 user manual; www.prensilia.com/portfolio/ih2-azzurra/.
76. T. E. Wiste, S. A. Dalley, T. J. Withrow, M. Goldfarb, in *2009 IEEE International Conference on Rehabilitation Robotics* (IEEE, Kyoto, Japan, 2009), pp. 675–681.

Acknowledgments: We thank the volunteers who participated in the study; A. Veronelli for contribution to the mechanical design in the initial phase of the project; A. F. Kleppa, A. Marinelli, S. Scarpetta, and A. Cimolato for support in conducting the experiments and the production of the material; V. Squeri, M. L. D'Angelo, and P. Randi for help in the clinical trials; F. Tessari for support in revising the mechatronics section; M. Chiappalone and G. Barresi for valuable advice on writing the paper; G. Berretta, S. Stedman, and D. Farina for the support in the preparation of the videos. We also thank M. Zambelli for key advice on the development and revision of the device and L. De Bartolomeis, G. Diamanti, and F. Poli for support in the industrial design of the device. **Funding:** This work was supported by the INAIL under grant agreement PPR1A. **Author contributions:** M.L. conceived and designed the study and coordinated the scientific and technical aspects of this work. N.B. conducted the mechatronic integration, tested the device, and performed all the clinical trials. S.T. conducted the mechanical development of the systems. L.L. developed part of the electronics and conducted the PCA. M.C. developed the electronics. A.L. conducted the mechanical development of the systems and coordinated the mechanical engineering team in the final phase of the project. M.S. analyzed the outcome of the clinical trials. A.N. coordinated the "Human-like synergistic behavior" experiments. J.A.S. conceived and designed the study and co-coordinated the project with M.L. in its initial phase. R.S. was clinical and technical advisor. E.G. was clinical and technical advisor and coordinated the clinical trials. L.D.M. conceived and designed the study and revised the work. M.L., L.L., A.L., M.S., and A.N. wrote the manuscript. N.B. and S.T. contributed to the writing of the paper. N.B., M.S., A.N., L.L., and S.T. prepared the figures; N.B., A.N., and E.G. prepared the videos. M.L. and L.D.M. revised the manuscript and coordinated the review process. M.L., J.A.S., and L.D.M. supervised the teams involved in the study and collected the funding to perform the study. All the authors have read and approved the manuscript in its final form. **Competing interests:** M.L., N.B., S.T., A.L., E.G., and L.D.M. are listed as inventors in the following patent applications: PCT application no. PCT/IB2019/052172 "Artificial Wrist"; PCT application no. PCT/IB2019/053682 "An Underactuated Prosthetic Hand"; PCT application no. PCT/IB2019/053683 "Prosthetic Finger"; and PCT application no. PCT/IB2019/056142 "Prosthetic Wrist" submitted by the Istituto Italiano di Tecnologia and INAIL, which cover the fundamental principles and design of Hannes. The other authors declare that they have no competing interests. **Data and materials availability:** All data and materials are available in the main text or the Supplementary Materials.

Submitted 25 January 2020
Accepted 18 August 2020
Published 23 September 2020
10.1126/scirobotics.abb0467

Citation: M. Laffranchi, N. Boccardo, S. Traverso, L. Lombardi, M. Canepa, A. Lince, M. Semprini, J. A. Saglia, A. Naceri, R. Sacchetti, E. Gruppioni, L. De Michieli, The Hannes hand prosthesis replicates the key biological properties of the human hand. *Sci. Robot.* **5**, eabb0467 (2020).

Science Robotics

The Hannes hand prosthesis replicates the key biological properties of the human hand

M. Laffranchi, N. Boccardo, S. Traverso, L. Lombardi, M. Canepa, A. Lince, M. Semprini, J. A. Saglia, A. Naceri, R. Sacchetti, E. Gruppioni, and L. De Michieli

Sci. Robot. **5** (46), eabb0467. DOI: 10.1126/scirobotics.abb0467

Science Robotics (ISSN 2470-9476) is published by the American Association for the Advancement of Science. 1200 New York Avenue NW, Washington, DC 20005. The title *Science Robotics* is a registered trademark of AAAS.